

# Koopman-based Control for Stochastic Systems: Application to Enhanced Sampling

Lei Guo<sup>\*,\*\*</sup> Jan Heiland<sup>\*\*\*</sup> Feliks Nüske<sup>\*</sup>

<sup>\*</sup> *Max-Planck-Institute for Dynamics of Complex Technical Systems,  
Magdeburg, Germany*

<sup>\*\*</sup> *Otto von Guericke Universität Magdeburg, Germany*

<sup>\*\*\*</sup> *Technische Universität Ilmenau, Germany*

---

**Abstract:** We present a data-driven approach to use the Koopman generator for prediction and optimal control of control-affine stochastic systems. We provide a novel conceptual approach and a proof-of-principle for the determination of optimal control policies which accelerate the simulation of rare events in metastable stochastic systems.

*Keywords:* metastability, Koopman generator, bi-linear, control affine, optimal control

---

## 1. INTRODUCTION

Stochastic dynamics with metastability are a recurring theme in many scientific disciplines, for instance, in simulations of macro-molecules, in climate systems, and in applications of uncertainty quantification. Metastability describes the existence of long-lived macro-states in a dynamical system's state space, such that transitions between these macro-states are rare events.

As is well known, metastability can be quantified using the dominant spectrum of the associated Koopman operator [Davies (1982); Dellnitz and Junge (1999); Schütte et al. (1999)]. Numerical methods for spectral approximation of the Koopman operator based on variational principles [Noé and Nüske (2013)] and the extended dynamic mode decomposition (EDMD) algorithm [Williams et al. (2015a)] have been developed in recent years [Klus et al. (2018b)]. On the other hand, metastability is also closely related to control systems. There is a wide range of biased sampling algorithms, which seek to overcome the rare event nature of the dynamics using a time-dependent input, see e.g. [Mehdi et al. (2024)] for a recent review. In fact, the exit time from a metastable state can be written as the value function of a specific stochastic optimal control problem [Hartmann et al. (2017)].

In this study, we join the ideas of Koopman-based modeling and biased sampling. The key ingredient is the generator extended dynamic mode decomposition algorithm (gEDMD) [Klus et al. (2020)], a variant of EDMD to approximate the Koopman generator. It was shown in [Peitz et al. (2020)] that for control-affine stochastic differential equations (SDEs), application of gEDMD reduces the Kolmogorov backward equation into an ODE that is bi-linear in expectation and input. This simplified structure can be

utilized for designing controllers which are geared towards accelerated sampling of rare events.

This paper is a first proof-of-principle that the gEDMD method for control-affine SDEs can be used to a) accurately predict the expectation of observable functions of interest for fixed control input; b) solve optimal control problems (OCPs) with integrated running cost and terminal cost; c) design OCPs which enforce accelerated transitions between metastable states. The paper is organized as follows: Section 2 provides a brief introduction to Koopman operators for (controlled) stochastic systems, the gEDMD method, and its application to optimal control problems. Section 3 presents the numerical results for various cost functions in OCPs. The conclusion is located in Section 4.

## 2. KOOPMAN THEORY FOR CONTROL-AFFINE SYSTEMS

### 2.1 Stochastic Systems and Koopman Operators

*Stochastic Differential Equations (SDEs)* We start by considering a time-homogeneous stochastic differential equation

$$dX_t = b(X_t)dt + \sigma(X_t)dW_t, \quad X_0 =: x \quad (1)$$

with the state  $X_t \in \mathbb{R}^n$ , the drift vector field  $b: \mathbb{R}^n \rightarrow \mathbb{R}^n$ , the diffusion matrix field  $\sigma: \mathbb{R}^n \rightarrow \mathbb{R}^{n \times s}$  and the Brownian motion  $(W_t)_{t \geq 0}$  in  $\mathbb{R}^s$ . Moreover, to guarantee the global existence of solutions to (1), we assume that  $b, \sigma$  satisfy standard Lipschitz properties [Thm.5.2.1 in Øksendal (2003)].

*Koopman Operators* The stochastic Koopman operator  $\mathcal{K}^t: \mathcal{L}^\infty(\mathbb{R}^n) \rightarrow \mathcal{L}^\infty(\mathbb{R}^n)$ , associated with an observable  $g: \mathbb{R}^n \rightarrow \mathbb{C}$ , is defined in, e.g. [Mezić (2005)] as follows

$$\mathcal{K}^t g(x) = \mathbb{E}^x(g(X_t)), \quad (2)$$

where  $\mathbb{E}^x(\cdot)$  denotes the conditional expectation given an initial value  $x$ . The generator  $\mathcal{L}$  with its domain  $\mathcal{D}(\mathcal{L})$  of the stochastic Koopman operator  $\mathcal{K}^t$  is defined by

---

\* Lei Guo is supported by Deutsche Forschungsgemeinschaft through Research Training Group 2297 "Mathematical Complexity Reduction" (MathCoRe).

$$\mathcal{L}\phi := \lim_{t \rightarrow 0} \frac{\mathcal{K}^t \phi - \phi}{t}, \quad \forall \phi \in \mathcal{D}(\mathcal{L}).$$

It can be shown by using Ito's lemma (see Section 4.4.2 of [Evans (2012)]) that  $\mathcal{L}$  acts as a second-order differential operator, i.e.

$$\mathcal{L}\phi = b\nabla_x \phi + \frac{1}{2}\Sigma : \nabla_x^2 \phi, \quad (3)$$

where the diffusion matrix is given by  $\Sigma := \sigma\sigma^T \in \mathbb{R}^{n \times n}$  and  $:$  is the Frobenius inner product. Semigroup theory implies that the conditional expectation is the solution of so-called backward Kolmogorov equation, i.e.

$$\frac{\partial}{\partial t} \mathbb{E}^x(\phi(X_t)) = \mathcal{L}\mathbb{E}^x(\phi(X_t)) \quad (4)$$

with the initial value  $\mathbb{E}^x(\phi(X_0)) = \phi(x)$ .

*Koopman Generator for Controlled SDEs* Now, consider a controlled stochastic differential equation with control-affine drift defined by

$$dX_t = (b(X_t) + \sum_{i=1}^p G_i(X_t)u_i(t))dt + \sigma(X_t)dW_t, \quad (5)$$

where  $u: \mathbb{R}_{\geq 0} \rightarrow \mathbb{R}^p$  is the input signal and  $G_i: \mathbb{R}^n \rightarrow \mathbb{R}^n$ ,  $i = 1, \dots, p$ , are Lipschitz continuous vector fields. The Koopman generator for such systems, derived from (3), is given as follows:

$$\mathcal{L}_u \phi = (b + \sum_{i=1}^p G_i u_i(t))\nabla_x \phi + \frac{1}{2}\Sigma : \nabla_x^2 \phi. \quad (6)$$

As in (4), the operator  $\mathcal{L}_u$  evolves the following partial differential equation (see Section III of Fleming and Soner (2006)):

$$\frac{\partial}{\partial t} \mathbb{E}^x(\phi(X_t)) = \mathcal{L}_u \mathbb{E}^x(\phi(X_t)), \quad \mathbb{E}^x(\phi(X_0)) = \phi(x). \quad (7)$$

Note that (7) is now a time-inhomogeneous equation.

## 2.2 Learning Methods

To perform numerical calculations on the Koopman generator, one can compute a Galerkin projection onto a finite dimensional space  $\mathcal{F} = \text{span}\{\psi_i\}_{i=1}^N$ , spanned by a finite basis of observable functions. As shown in [Klus et al. (2020)], the matrix representation of this Galerkin projection is

$$L = AC^\dagger,$$

with the stiffness and mass matrices

$$A_{ij} = \langle \mathcal{L}\psi_i, \psi_j \rangle_\mu, \quad C_{ij} = \langle \psi_i, \psi_j \rangle_\mu.$$

Here,  $\mu$  is a probability measure, which is typically chosen as an invariant measure in the time-homogeneous case. Moreover, if we have a data set  $X = \{x_l\}_{l=1}^m$  of samples from  $\mu$ , we can compute empirical estimators for the stiffness and mass matrices.

To this end, we introduce vector valued functions  $\Psi: \mathbb{R}^n \rightarrow \mathbb{C}^N$  and  $\mathcal{L}\Psi: \mathbb{R}^n \rightarrow \mathbb{C}^N$  as

$$\Psi(\mathbf{x}) = \begin{pmatrix} \psi_1(\mathbf{x}) \\ \vdots \\ \psi_N(\mathbf{x}) \end{pmatrix}, \quad \mathcal{L}\Psi(\mathbf{x}) = \begin{pmatrix} \mathcal{L}\psi_1(\mathbf{x}) \\ \vdots \\ \mathcal{L}\psi_N(\mathbf{x}) \end{pmatrix}.$$

Likewise, we make the definitions

$$\begin{aligned} \Psi(X) &= [\Psi(x_1) \cdots \Psi(x_m)] \in \mathbb{C}^{N \times m}, \\ \mathcal{L}\Psi(X) &= [\mathcal{L}\Psi(x_1) \cdots \mathcal{L}\Psi(x_m)] \in \mathbb{C}^{N \times m}. \end{aligned}$$

Then the empirical estimators for the mass and stiffness matrix are given by

$$\hat{A} = \frac{1}{m} \mathcal{L}\Psi(X)\Psi(X)^H, \quad \hat{C} = \frac{1}{m} \Psi(X)\Psi(X)^H.$$

The final empirical matrix approximation of Koopman generator is given by

$$\hat{L} = \hat{A} \left( \hat{C} + \lambda \text{Id} \right)^\dagger,$$

where  $\lambda \geq 0$  is a regularization parameter. This estimation method is called generator extended dynamic mode decomposition (gEDMD) [Klus et al. (2020)].

*Prediction with gEDMD* Furthermore, if we assume that  $\mathbb{E}^x(\phi(X_t)) \in \mathcal{F}$  for  $\phi \in \mathcal{F}$ , i.e.

$$\mathbb{E}^x(\phi(X_t)) = \sum_{i=1}^N v_i(t)\psi_i(x) = V(t)^H \Psi(x) \quad (8)$$

with time-dependent vector  $V(t) = (v_1(t), \dots, v_N(t))^T$ , then (4) turns into

$$\frac{\partial}{\partial t} V(t)^H \Psi(x) = V(t)^H \mathcal{L}\Psi(x),$$

which implies that the time evolution of the expectation satisfies a data-driven linear ODE on the finite-dimensional space  $\mathcal{F}$ , i.e.

$$\frac{d}{dt} V(t)^H = V(t)^H \hat{L}. \quad (9)$$

*Bi-linear ODE for Control-affine Systems* For a time-dependent system such as (5), constructing the empirical generator approximation becomes quite challenging because, according to (7),  $\mathcal{L}_u \psi_k(x)$  depends not only on the data but also on the time-dependent input signal  $u(t)$ . If we consider constant inputs

$$u \in \mathcal{U} = \{0, e_1, \dots, e_p\},$$

where  $e_i \in \mathbb{R}^p$  for  $i = 1, \dots, p$  are unit vectors, then the generators corresponding to these constant inputs are given by

$$\mathcal{L}_0 = b\nabla_x + \frac{1}{2}\Sigma : \nabla_x^2, \quad \mathcal{L}_{e_i} = (b + G_i)\nabla_x + \frac{1}{2}\Sigma : \nabla_x^2$$

which, based on (6), results in

$$\mathcal{L}_u = \mathcal{L}_0 + \sum_{i=1}^p (\mathcal{L}_{e_i} - \mathcal{L}_0)u_i(t). \quad (10)$$

That is, the control-affine drift leads to a control-affine Koopman generator [Peitz and Klus (2019)]. Consequently, the evolution equation (7) can be written as follows

$$\begin{cases} \frac{\partial}{\partial t} \mathbb{E}^x(\phi(X_t)) = (\mathcal{L}_0 + \sum_{i=1}^p (\mathcal{L}_{e_i} - \mathcal{L}_0)u_i(t))\mathbb{E}^x(\phi(X_t)), \\ \mathbb{E}^x(\phi(X_0)) = \phi(x). \end{cases} \quad (11)$$

For given data set  $X$ , vector valued function  $\Psi$  and input signal  $u(t)$ , the empirical matrix approximations of generators with constant inputs  $L_0$  and  $L_{e_i}$  for  $i = 1, \dots, p$  can be obtained by applying gEDMD as outlined in Alg.1.

Hence, by (10), the matrix approximation of the control-affine generator is likewise given by

$$L_u = L_0 + \sum_{i=1}^p (L_{e_i} - L_0) u_i.$$

Under the assumption (8), and by a similar derivation as for (9), the PDE (11) can be approximated by the following bi-linear ODE

$$\frac{d}{dt} V(t)^H = V(t)^H L_u. \quad (12)$$

---

**Algorithm 1** gEDMD for Control-Affine Systems

---

**Input:**  $X = (x_1, x_2, \dots, x_m) \in \mathbb{R}^{n \times m}$   
 $\Psi = (\psi_1, \dots, \psi_N)^\top$ ,  $u(\cdot) \in \mathbb{R}^p$ ,  $\lambda \geq 0$   
**Output:**  $L_0, L_{e_i}, L_u \in \mathbb{C}^{N \times N}$  for  $i = 1, \dots, p$

- 1:  $C = \Psi(X)\Psi(X)^H$
- 2: Set  $G_0 = 0$  and  $e_0 = 0$ .
- 3: **for**  $i = 0, \dots, p$  **do**
- 4:  $A_{e_i} = \mathcal{L}_{e_i} \Psi(X)\Psi(X)^H$
- 5:  $L_{e_i} = A_{e_i} (C + \lambda \text{Id})^\dagger$
- 6: **end for**
- 7:  $L_u = L_0 + \sum_{i=1}^p (L_{e_i} - L_0) u_i$

---

*Random Fourier Features* Numerous options exist for choice of basis functions  $\{\psi_i\}_{i=1}^N$ , e.g. Hermite polynomials and radial basis functions (RBFs) [Williams et al. (2015a)]. In order to generate expressive basis sets while keeping the number of parameters manageable, kernel-based methods relying on reproducing kernel Hilbert spaces (RKHS), see e.g. [Section 4 of Christmann and Steinwart (2008)], have been proposed as discussed in [Williams et al. (2015b), Klus et al. (2018a)]. The random Fourier features (RFFs) outlined in [Rahimi and Recht (2007)] can then be used to efficiently approximate these kernel functions.

We consider a translation invariant kernel  $k$  on  $\mathbb{X} = \mathbb{R}^n$ , which satisfies  $k(x, x) = 1$ . Then, Bochner's theorem guarantees that the kernel is indeed the Fourier transformation of a finite positive Borel probability measure  $\rho$  on  $\mathbb{R}^n$ , i.e.

$$k(x, y) = \mathbb{E}_{\omega \sim \rho} (e^{-ix^\top \omega} e^{-iy^\top \omega}).$$

To approximate the kernel, we define the random Fourier feature (RFF) mapping  $\phi_{\text{RFF}}: \mathbb{R}^n \rightarrow \mathbb{C}^N$  by

$$\phi_{\text{RFF}}(x) = \begin{pmatrix} \phi_1(x) \\ \vdots \\ \phi_N(x) \end{pmatrix} = \begin{pmatrix} e^{ix^\top \omega_1} \\ \vdots \\ e^{ix^\top \omega_N} \end{pmatrix}, \quad (13)$$

where  $\{\omega_i\}_{i=1}^N$  are sampled from the spectral measure  $\rho$ . The point-wise approximation to the kernel  $k$  is then given as  $k(x, y) = \frac{1}{p} \phi_{\text{RFF}}(x)^H \phi_{\text{RFF}}(y)$ . As explained in [Nüske and Klus (2023)], approximating kernelized gEDMD by random Fourier features is equivalent to just using standard gEDMD with the randomly generated basis set  $\phi_{\text{RFF}}$ . That is the approach we follow in this paper.

### 2.3 Solution of the Control Problem

Our overall goal in this work is to find an optimal input  $u^*$  on the time horizon  $[0, T]$  such that it solves a nonlinear optimal control problem (OCP) of the form:

$$\begin{aligned} \min_{u: [0, T] \rightarrow \mathbb{R}^p} \quad & J(x, u), \\ \text{s.t.} \quad & \text{the dynamics (5),} \\ & \text{with } X_0 = x. \end{aligned} \quad (14)$$

The cost functional we consider is typically of the form:

$$J(x, u) := \mathbb{E}^x \left\{ \int_0^T l(X_t, u(t)) dt + \mathcal{T}(X_T) \right\},$$

where  $l(\cdot, \cdot)$  and  $\mathcal{T}(\cdot)$  are the running cost and the terminal cost, respectively. We only consider separable running costs of the form

$$l(X_t, u(t)) = l_1(X_t) + l_2(u(t)).$$

and we approximate the time integral using the piecewise trapezoidal rule. The expectations can then be approximated using gEDMD, if we treat the expectations as the solutions to the PDE (11) with the observables  $l_1(\cdot)$  and  $\mathcal{T}(\cdot)$ . To this end, the observables  $l_1$ ,  $\mathcal{T}$  must be contained in  $\mathcal{F}$ , i.e. there are coefficient vectors such that

$$l_1(x) = V_{l_1}^H \Psi(x), \quad \mathcal{T}(x) = V_{\mathcal{T}}^H \Psi(x).$$

Using Alg. 1 to provide a matrix approximation of the control-affine generator  $L_u$ , and based on the assumption (8), the approximated expectations  $\mathbb{E}^x(l_1(X_t))$  and  $\mathbb{E}^x(\mathcal{T}(X_t))$  can be computed by solving the bi-linear ODE (12) with the initial conditions  $V_{l_1}(0) = V_{l_1}$  and  $V_{\mathcal{T}}(0) = V_{\mathcal{T}}$ , respectively. We note that if we are only looking to solve (14) for a single initial position  $x$ , it is more efficient to solve a dual problem instead. Denoting the flow map of the ODE (12) by  $\Phi_u^t$ , then for any any observable  $\phi \in \mathcal{F}$ , we have

$$\mathbb{E}^x[\phi(X_t)] = (\Phi_u^t(V_\phi(0)))^H \Psi(x).$$

For fixed  $u$ , the ODE (12) is a linear time-dependent equation, and hence the flow map  $\Phi_u^t$  is also linear. It follows that

$$\mathbb{E}^x[\phi(X_t)] = V_\phi(0)^H (\Phi_u^t)^H \Psi(x) = V_\phi(0)^H \gamma(t),$$

where  $\gamma(t) := (\Phi_u^t)^H \Psi(x)$  is the solution to the adjoint equation

$$\frac{d}{dt} \gamma(t)^H = \gamma(t)^H L_u^H,$$

with the initial condition  $\gamma(0)^H = \Psi(x)^H$ . Putting these pieces together, we can evaluate the cost functional  $J(x, u)$  for any input signal  $u$ . The optimization is then carried out using a black-box solver from the *scipy* library.

## 3. RESULTS

In this section, we perform numerical simulations using the following one-dimensional SDE with control-affine drift, given by

$$dX_t = -(\nabla V(X_t) + K_{\text{bias}}(X_t - u(t))) dt + \sqrt{2\beta^{-1}} dW_t \quad (15)$$

with the double-well potential  $V: \mathbb{R} \rightarrow \mathbb{R}$  defined as

$$V: x \mapsto K_{\text{dw}}(x^2 - 1)^2. \quad (16)$$

Here,  $K_{\text{dw}}$ ,  $K_{\text{bias}}$ ,  $\beta \in \mathbb{R}_{>0}$ , are constants, and  $u: [0, T] \rightarrow \mathbb{R}$  is the input signal. The diffusion constant  $\beta$  is called inverse temperature in statistical physics, we set  $\beta = 1$  in all numerical experiments. For training, we use the constant inputs  $u \in \{-1, 1\}$ . Note that the corresponding drift fields are the derivatives of quadratic bias energies

$$B_1 := \frac{K_{\text{bias}}}{2}(x+1)^2, \quad B_2 := \frac{K_{\text{bias}}}{2}(x-1)^2,$$

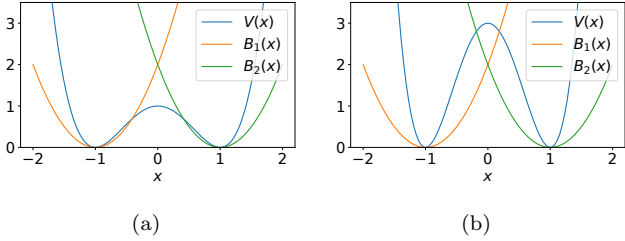


Fig. 1. Double-well potential  $V$  and bias energies  $B_i$  with  $K_{\text{bias}} = 4$  for  $K_{\text{dw}} = 1$  (a) and  $K_{\text{dw}} = 3$  (b)

which are used in many adaptive sampling algorithms. Also, note that we do not learn a model for the generator  $\mathcal{L}_0$  of the metastable physical system, but use two dynamics with localized energy functions instead.

### 3.1 Prediction

As a first application of the bi-linear gEDMD framework, we consider a fixed input  $u(\cdot)$ , and use gEDMD to predict the expectation of observable functions along the trajectory of the dynamics. For the double-well example, we choose the input as a periodic signal  $u(t) := \cos(2t)$ . We set the initial condition  $x = 0.5$ , the step size  $\Delta t = 10^{-3}$  and the number of steps  $N_s = 5 \times 10^3$ . Additionally, we use random Fourier features  $\phi_{\text{RFF}}$  (13) to span the finite-dimensional subspace, where  $\{\omega_i\}_{i=1}^N$  are sampled from the spectral density of a Gaussian kernel with the bandwidth 0.5, and the number of features is set to  $N = 50$ . Furthermore, the training data  $\{x_l\}_{l=1}^m$  are  $m$  points uniformly distributed on the interval  $[-2, 2]$ . On these data, we learn the matrix models for the generators  $\mathcal{L}_{-1}$  and  $\mathcal{L}_1$  for the constant inputs  $u = -1$  and  $u = 1$ , respectively.

Using the bi-linear dynamics (12), we compute an approximation  $\hat{\mathbb{E}}^x(X_t)$  to the true expectation  $\mathbb{E}^x(X_t)$  of the dynamics (15). As a ground truth for  $\mathbb{E}^x(X_t)$ , we compute empirical averages over 100 trajectories, generated by the Euler-Maruyama scheme. We denote the absolute value of the prediction error by

$$|e(t)| := |\mathbb{E}^x(X_t) - \hat{\mathbb{E}}^x(X_t)|.$$

We investigate how the constants  $K_{\text{dw}}$ ,  $K_{\text{bias}}$ , the regularization parameter  $\lambda$  and the size of the training data  $m$  affect the absolute error  $|e(t)|$ . In addition, we consider the prediction as a failure if  $|e(t)| \geq 1$  for any  $t$ . We omit failed predictions when computing mean errors for  $e(t)$ , but we also report the success rate  $\delta$ .

Fig. 2 shows how the error  $|e(t)|$  (panels a&b) and the success rate (panels c&d) vary with the data size for each value of  $K_{\text{dw}} = \{1, 2, 3\}$ , regularization parameters  $\lambda \in \{0, 10^{-10}\}$ , while keeping either the biasing constant at  $K_{\text{bias}} = 3$  or at  $K_{\text{bias}} = 4$ . We observe that the predictions are very reliable for  $K_{\text{dw}} \in \{1, 2\}$ , and more susceptible to instabilities for the more metastable system  $K_{\text{dw}} = 3$ . We notice that for this latter case, using no regularization  $\lambda = 0$  works better for  $K_{\text{bias}} = 3$ , while a small amount of regularization  $\lambda = 10^{-10}$  seems appropriate for  $K_{\text{bias}} = 4$ .

As a consequence, we will use the settings  $(K_{\text{bias}}, \lambda) = (3, 0)$  and  $(K_{\text{bias}}, \lambda) = (4, 10^{-10})$ , and only moderate training data sizes around  $m = 10^3$ , in all of the following examples. A more detailed study of the interplay between

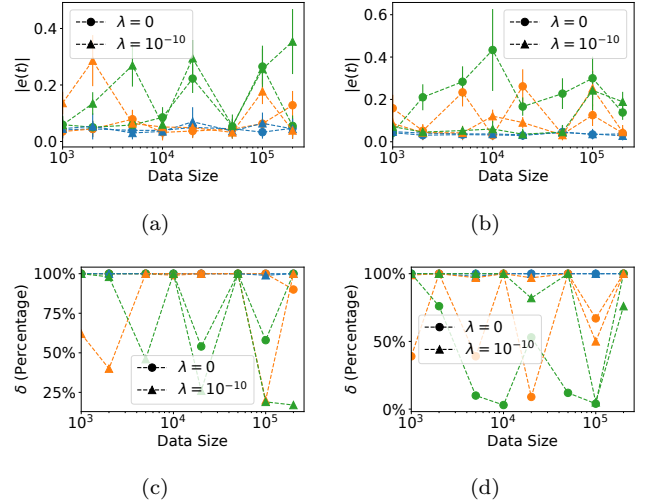


Fig. 2. Absolute prediction errors (top row) and success rates  $\delta$  (bottom row) with  $K_{\text{bias}} = 3$  (left) and  $K_{\text{bias}} = 4$  (right). Blue, orange and green lines stand for the cases when  $K_{\text{dw}} = \{1, 2, 3\}$  respectively.

basis set size  $N$ , data size  $m$ , and regularization parameter  $\lambda$  is planned for the future.

### 3.2 Tracking

We now consider a more complex problem: steering the expectation to a predefined value. This can be formulated as an optimization problem. Given a reference signal  $x_{\text{ref}}: [0, T] \rightarrow \mathbb{R}$ , the goal is to find an optimal input control  $u^*$  that solves the following finite horizon optimization problem:

$$\begin{aligned} \min_{u: [0, T] \rightarrow \mathbb{R}} \quad & \int_0^T \|\mathbb{E}^x(X_t) - x_{\text{ref}}(t)\|^2 dt \\ \text{s.t.} \quad & \text{the dynamics (15),} \\ & \text{with } X_0 = x. \end{aligned} \quad (17)$$

We define the absolute tracking error as

$$|e_t(t)| := |\mathbb{E}^x(X_t) - x_{\text{ref}}(t)|,$$

while the reference signal is  $x_{\text{ref}}(t) = \cos(2t)$ , i.e. the same signal that was used as fixed input before. We consider four different settings for the system parameter  $K_{\text{dw}}$ , the biasing strength  $K_{\text{bias}}$ , and the regularization parameter  $\lambda$ , namely  $(K_{\text{dw}}, K_{\text{bias}}, \lambda) \in \{(1, 3, 0), (3, 3, 0), (1, 4, 10^{-10}), (3, 4, 10^{-10})\}$ . We set the data size to  $m = 10^3$  and the final time to  $T = 2$ , thus tracking the reference signal for one complete transition from the left to the right minimum. The remaining parameter values are the same as those specified in the previous section.

For four settings, we show in the first row of Fig. 3, the piecewise continuous solution  $u^*$  and the absolute error  $|e_t|$ . The corresponding tracking performances are shown in the second row of Fig. 3. As the initial condition  $x$  and  $x_{\text{ref}}(0)$  are not identical, we omit the time interval  $[0, 0.1]$ , during which the controlled system catches up with the reference, in the first row.

The results demonstrate that  $\mathbb{E}^x(X_t)$  effectively tracks the reference  $x_{\text{ref}}(t)$  over the time interval  $[0, 2]$  in all cases.

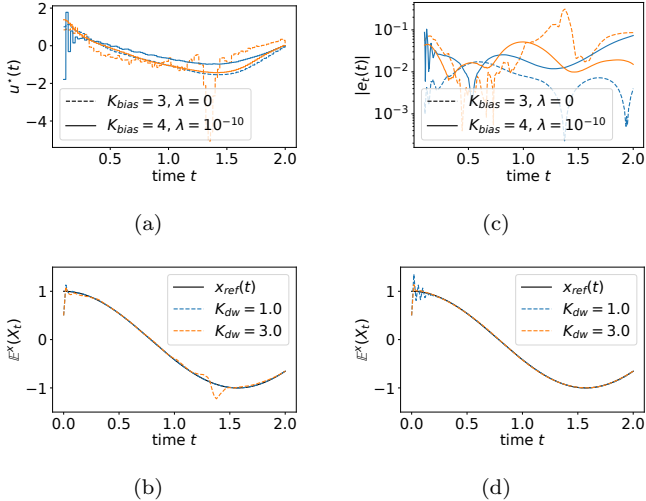


Fig. 3. Numerical results for the tracking optimal control problem (17). (a)&(c) are the optimal signals and tracking errors for four parameter settings. Blue and orange lines stand for the systems when  $K_{dw} \in \{1, 3\}$ , respectively. Panels (b)&(d) are the tracking performances for fixed  $K_{bias} = 3$  and  $K_{bias} = 4$ , respectively.

For the systems with  $K_{dw} = 1$ , accurate tracking is easily achieved. We only observe that for  $K_{bias} = 4, \lambda = 10^{-10}$ , the optimal solution displays some oscillations around the reference initially, while for  $K_{bias} = 3, \lambda = 0$ , the tracking error is limited to less than one per cent for most of the control horizon. For the second, more strongly metastable system with  $K_{dw} = 3$ , the solution for  $K_{bias} = 3, \lambda = 0$  allows for some stronger oscillation, while the tracking error of the system with  $K_{bias} = 4, \lambda = 10^{-10}$  is limited to less than 10 per cent throughout.

### 3.3 Loss Functions for Enhanced Sampling

In this section, we explore the use of optimal control to accelerate transitions between metastable states. For the double-well potential (16), which has two metastable minima at  $x = -1$  and  $x = 1$ , we consider the problem of enforcing a transition from the left minimum to the right basin. That is, with the initial condition  $x = -1$ , we aim to solve the optimal control problem (14) with the cost defined as

$$J(x, u) := \mathbb{E}^x \left\{ \int_0^T l(X_t, u(t)) dt \right\} + (1 - \mathbb{E}^x \{X_T\})^2.$$

The terminal cost is chosen to ensure that the dynamics will approximately reach the right minimum at the final time  $T$ . We explore, for  $c \in \mathbb{R}_{>0}$ , two choices of the running cost: first,

$$l_{dw} := V(X_t) + c \|u(t)\|^2, \quad (18)$$

which penalizes the potential energy and the magnitude of the input  $u$ . Another meaningful choice of running cost is

$$l_{bias} := V(X_t) + c \|X_t - u(t)\|^2, \quad (19)$$

which exerts a penalty on both the physical energy and the bias energy spent during the simulation. We study four different system settings, namely  $(K_{dw}, K_{bias}) \in \{(1, 3), (1, 4), (3, 3), (3, 4)\}$ . Furthermore, we fix the size of

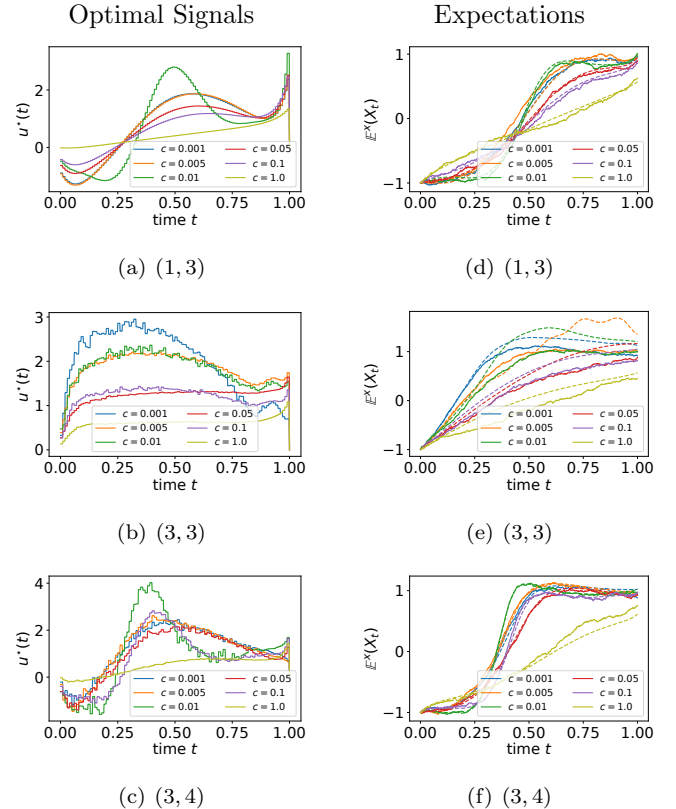


Fig. 4. Numerical results of the problem (14) for the running cost (18) with a range of parameters  $c$ . Left column are optimal signals and right column are expectations of the state  $\mathbb{E}^x(X_t)$ . From top to bottom are the results for the settings  $(K_{dw}, K_{bias}) \in \{(1, 3), (3, 3), (3, 4)\}$ , respectively, we omit the combination (1, 4) as it is very similar to the first row. Solid and dashed lines stand for the reference and approximated expectations, respectively.

the training data as  $m = 10^3$  and the final time as  $T = 1$ . All remaining settings are the same as in section 3.1.

### 3.4 Comparison

For the four different system settings, we solve the optimization problems for a range of values of the parameter  $c$  between  $c = 10^{-3}$  and  $c = 2.0$ . The results are shown in Figs. 4 & 5. Generally speaking, the results for both loss functions and systems are fairly similar. We find that there is a parameter range with  $c$  between  $10^{-3}$  and  $10^{-1}$ , where the control objective of steering the system across the barrier is achieved. In most cases, the optimal signal displays a peak of the input signal, resulting in a rapid transition of the system state. The transition occurs a bit earlier for  $(K_{dw}, K_{bias}) = (3, 4)$  as opposed to  $(K_{dw}, K_{bias}) = (1, 3)$ . For the parameters  $(K_{dw}, K_{bias}) = (3, 3)$ , however, a more gradual transition is achieved by applying a rather flat input signal. We also notice once again that in almost all cases, the expected values predicted by the bi-linear gEDMD model perfectly match the empirical mean values obtained from simulating the controlled dynamics (5) with the optimal inputs signals  $u^*$ .

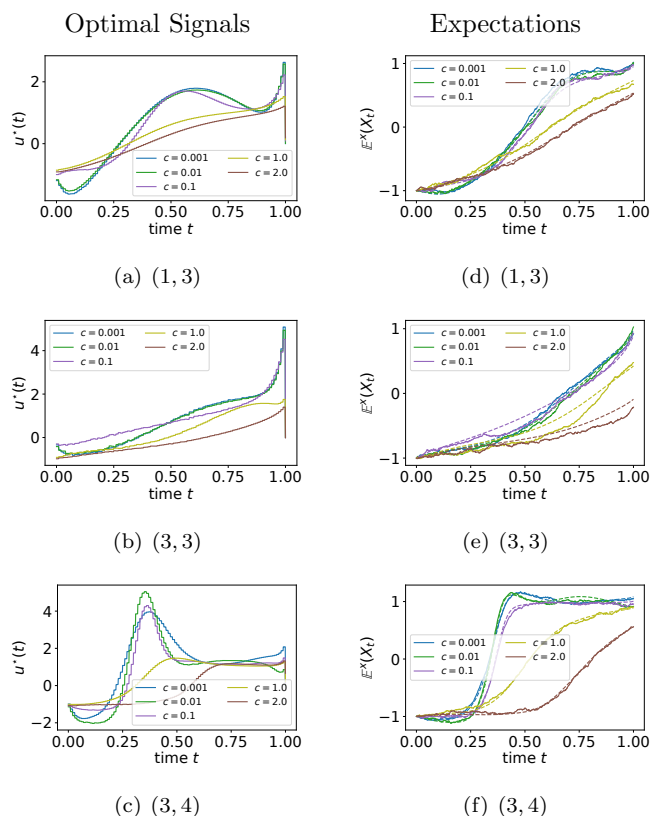


Fig. 5. Same as in Figure 4, but for the running cost (19).

#### 4. CONCLUSION

We have demonstrated the capabilities of the gEDMD algorithm for prediction and optimal control of control-affine stochastic systems. In particular, we have shown that optimal control policies for rare event sampling can be determined with limited amounts of data. Future research will explore the application of the method to more complex systems in higher dimensions, with a focus on the selection of training systems and generation of training data. We will also continue to investigate the efficient tuning of hyper-parameters, as well as the theoretical foundations of the method. We hope that our findings in this paper will inspire further research and practical applications in the field.

#### DATA AVAILABILITY STATEMENT

Codes and data to reproduce the results and figures shown in this manuscript are available from the following public repository:

<https://doi.org/10.5281/zenodo.13838629>

#### REFERENCES

Christmann, A. and Steinwart, I. (2008). *Support Vector Machines*. Springer New York.

Davies, E.B. (1982). Metastable States of Symmetric Markov Semigroups II. *Journal of the London Mathematical Society*, s2-26(3), 541–556.

Dellnitz, M. and Junge, O. (1999). On the approximation of complicated dynamical behavior. *SIAM J. Numer. Anal.*, 36(2), 491–515.

Evans, L.C. (2012). *An Introduction to Stochastic Differential Equations*, volume 82. American Mathematical Soc.

Fleming, W.H. and Soner, H.M. (2006). *Controlled Markov Processes and Viscosity Solutions*, volume 25. Springer-Verlag.

Hartmann, C., Richter, L., Schütte, C., and Zhang, W. (2017). Variational Characterization of Free Energy: Theory and Algorithms. *Entropy*, 19(11), 626.

Klus, S., Bittracher, A., Schuster, I., and Schütte, C. (2018a). A kernel-based approach to molecular conformation analysis. *The Journal of Chemical Physics*, 149(24).

Klus, S., Nüske, F., Koltai, P., Wu, H., Kevrekidis, I., Schütte, C., and Noé, F. (2018b). Data-Driven Model Reduction and Transfer Operator Approximation. *Journal of Nonlinear Science*, 28(3), 985–1010.

Klus, S., Nüske, F., Peitz, S., Niemann, J.H., Clementi, C., and Schütte, C. (2020). Data-driven approximation of the Koopman generator: Model reduction, system identification, and control. *Physica D: Nonlinear Phenomena*, 406.

Mehdi, S., Smith, Z., Herron, L., Zou, Z., and Tiwary, P. (2024). Enhanced sampling with machine learning. *Annual Review of Physical Chemistry*, 75(Volume 75, 2024), 347–370.

Mezić, I. (2005). Spectral Properties of Dynamical Systems, Model Reduction and Decompositions. *Nonlinear Dynamics*, 41(1-3), 309–325.

Noé, F. and Nüske, F. (2013). A variational approach to modeling slow processes in stochastic dynamical systems. *Multiscale Modeling and Simulation*, 11(2), 635–655.

Nüske, F. and Klus, S. (2023). Efficient approximation of molecular kinetics using random Fourier features. *The Journal of Chemical Physics*, 159(7), 074105.

Øksendal, B. (2003). *Stochastic Differential Equations*. Springer Berlin Heidelberg.

Peitz, S. and Klus, S. (2019). Koopman operator-based model reduction for switched-system control of PDEs. *Automatica*, 106, 184–191.

Peitz, S., Otto, S.E., and Rowley, C.W. (2020). Data-Driven Model Predictive Control using Interpolated Koopman Generators. *SIAM Journal on Applied Dynamical Systems*, 19(3), 2162–2193.

Rahimi, A. and Recht, B. (2007). Random features for large-scale kernel machines. *Advances in Neural Information Processing Systems*, 20.

Schütte, C., Fischer, A., Huisinga, W., and Deuffhard, P. (1999). A direct approach to conformational dynamics based on hybrid Monte Carlo. *J. Comput. Phys.*, 151(1), 146–168.

Williams, M.O., Kevrekidis, I.G., and Rowley, C.W. (2015a). A Data-Driven Approximation of the Koopman Operator: Extending Dynamic Mode Decomposition. *Journal of Nonlinear Science*, 25(6), 1307–1346.

Williams, M.O., Rowley, C.W., and Kevrekidis, I.G. (2015b). A Kernel-Based Method for Data-Driven Koopman Spectral Analysis. *Journal of Computational Dynamics*, 2(2), 247–265.